Investigation Into the Optical Emission of Features for Powder-bed Fusion Am Process Monitoring

Yingjie Zhang (arabinjasmine@scut.edu.cn)
South China University of Technology
Wentao Yan
Xiaojun Peng
Zhangdong Chen
Zimeng Jiang
Di Wang

Research Article

Keywords: powder-bed fusion (PBF), AM process monitoring, optical emission features, K-means clustering

Posted Date: August 2nd, 2021

DOI: https://doi.org/10.21203/rs.3.rs-727364/v1

Investigation into the optical emission of features for powder-bed fusion AM process monitoring

Yingjie Zhang[1], Wentao Yan[2], Xiaojun Peng[1], Zhangdong Chen[1], Zimeng Jiang[1], Di Wang[3*]

1. Shien-Ming Wu School of Intelligent Engineering, South China University of Technology, Guangzhou, China
2. Department of Mechanical Engineering, National University of Singapore, Singapore
3. School of Mechanical and Automotive Engineering, South China University of Technology, Guangzhou, China

Corresponding author email: mewdlaser@scut.edu.cn

Abstract

Process monitoring and control is an essential approach to improve additive manufacturing (AM) built quality. For the development of powder bed fusion (PBF) AM monitoring system, sensing process optical emission is a popular approach, as it provides rich information on melt pool condition which directly determines final part quality. However, the optical emission information is convoluted. And the lack of full understanding of it limits the further development of an optimal monitoring system. Therefore, the aim of this study is to explore the correlations between the optical emission and the processing condition to help enhance PBF process monitoring. A high-speed camera was used to acquire the images of the optical emission in the waveband of 800 nm – 1,000 nm. Several typical features were extracted and analyzed with the increase of laser power. The *K*-means clustering method was used to identify the hidden patterns of these features. The SVM model was built for quality identification. Five process patterns have been identified and therefore the collected dataset was partitioned into five subsets. The extracted features in each subset was characterized. It is found that plume area and plume orientation are the two most crucial features for processing condition monitoring. Number of spatters and spatter dispersion index are sensitive to some minor process vibrations which have little effect on built quality. Additionally, the time sequence information of the features can help improve the quality identification performance.

Keywords: powder-bed fusion (PBF), AM process monitoring, optical emission features, K-means clustering

1. Introduction

Powder bed fusion (PBF) process monitoring has attracted great attention recently due to the requirement of reliability and repeatability on AM parts quality for functional use [1-3]. Optical emission contains rich information on melt pool, plume and spatter, which is closely related to processing conditions. Therefore, sensing the optical emission presents a great potential for an effective monitoring system development. Based on an "co-axial" monitoring system [4], the optical intensity measured by a photodiode as well as the melt pool features, e.g. melt pool area,

melt pool length and melt pool width, extracted from imaging measurements were demonstrated effective for internal voids detection [5, 6]. Grasso et al. [7] used an off-axial imaging measurement system and extracted a statistical descriptor based on principal component analysis applied to the detected image and indicated it was suitable for defective areas identification. Later, they also extracted the spatter- and plume-related features based on a thermal imaging system and showed their feasibility for process condition identification [8, 9]. Zhang et al. [10] compared the capability of features corresponding to different objects, melt pool, plume and spatter on process condition identification in virtue of machine learning methods. They found that the features corresponding to different objects were sensitive to different kinds of process anomalies. Montazeri et al. [11] studied the differences on overhang processing condition detection by using the features extracted from different sensors, including a photodetector, a high-speed visible camera and a short wave infrared thermal camera. They concluded that the features extracted from the short-wave infrared thermal camera showed the best classification performance. Scime et al. [12] extracted the melt pool signatures by computer vision techniques with "co-axial" measurement configuration. Based on unsupervised and supervised machine learning techniques they identified the melt pool signatures that may indicate flaws.

The studies demonstrated the feasibility of using optical emission information for AM process condition monitoring; meanwhile, they also revealed that the optical emission was convoluted. Sensing by different sensors, extracting different statistical descriptors or extracting features from different objects, are likely to affect the monitoring performance. Therefore, to enhance the monitoring system, the exploration of the relationships among the extracted features, the process parameters and process conditions is necessary. The PBF-process physical mechanism shows that the metal powders absorb the laser energy resulting in their temperature raise and melt is well known. Therefore, it is commonly believed that the melt pool features, e.g. melt pool area, melt pool length and melt pool width, are proportional to input energy, which is also verified by the AM process simulation [13, 14]. Analogously, the plume is caused by the melt pool surface vaporization, so that its image intensity and area are supposed to be proportional to the input laser energy as well. In terms of spatter related emission, up to now, no simulation model has been reported due to the complexity of spatter generation mechanism, while the spatter-related features were extracted and analyzed based on experimental measurements. For instance, Liu et al. [15] concluded that the energy input had a significant effect on spatter behavior, including spatter size, scattering state and jetting height. Gunenthiram et al. [16] found that with the increase of laser power, spatter ejected angle tended to be vertical to the scanning direction, and the spatter number increased except for the experimental conditions while in provoking balling.

In despite of this, the relationships mentioned above were established either based on the simulation models which were quite simplified as compared with the actual physical process or the actual observation of experimental samples, which cannot provide sufficient details on process condition identification. Several issues are still unclear, namely: 1) which are the most relevant features for built quality evaluation; 2) what are the differences between the information extracted from different objects/sensors; and 3) how does the optical emission changes along with the quality degradation.

Therefore, an in-depth investigation of the optical emission was conducted in this study. A high-speed camera was used for emission sensing. Several features were extracted from the

recorded images corresponding to different objects. The mean and variance of the features with the change of laser power were presented and interpreted. Furthermore, *K*-means clustering analysis technique was used as a method for grouping different features. The hidden patterns of features corresponding to the clusters were identified. The transformation of the patterns during quality degradation process were characterized. It is found that plume area and plume orientation are the two most relevant features for built quality evaluation. Number of spatters and dispersion index of spatters are sensitive to some light process vibrations which have little effect on built quality. Moreover, the time sequential information of the melt pool condition is crucial to determine the built quality.

2. Experimental Setup

The experiments were performed on our in-house developed machine equipped with a 200 W, 1,070 nm fiber laser, which is shown in Fig.1. The laser beam was focused by a focal lens. The material used was commercial AM stainless steel 316L powders with the particle size ranging from 10 μm to 45 μm. The single tracks were built under different energy inputs by varying laser power, as shown in Table 1. The layer thickness and laser beam diameter (or spot size) were consistent in this study, which were 80 μm and 100 μm, respectively. Fig.2 shows the built track morphologies corresponding to the parameters used in this work. According to the morphologies, the track samples were divided into two groups, "good" and "irregularity".

A Photron Fastcam Mini AX200 monochrome camera was used for process image acquisition. The full resolution of this camera is 1024 × 1024 pixels. The images were recorded with an off-axis camera setup with the sampling rate of 2,000 fps. The angle between the camera focal plane and the substrate surface was set as 45°. The lens with zoom of 12.5:1 and working distance of 135mm was configured. A 250 nm-800 nm cut-off filter was used to enhance the image contrast between the melt pool and the plume. This cut-off filter configuration enables the melt pool, plume and spatter to be easily identified in the recorded videos. The region of interest (ROI) with area of 12 × 5 mm^2 was used for video recording. This ROI area was selected based on our observation to ensure sufficient information can be obtained.

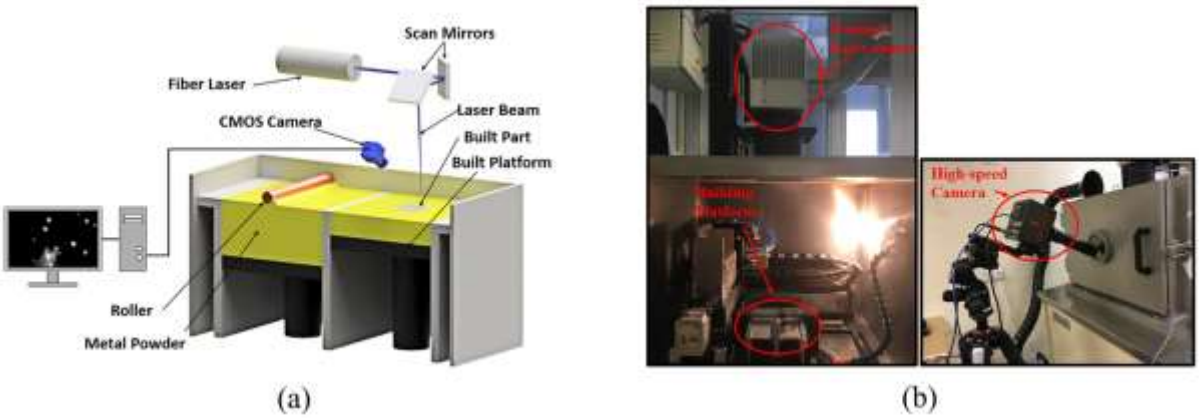

Fig. 1 Schematic of the experimental powder-bed fusion process monitoring system

Table 1: Single track built process parameters.

#	Laser power (W)	Scanning speed (mm/s)
1	70	100
2	80	100
3	90	100
4	100	100
5	110	100
6	120	100
7	130	100
8	140	100
9	150	100
10	160	100
11	170	100
12	180	100

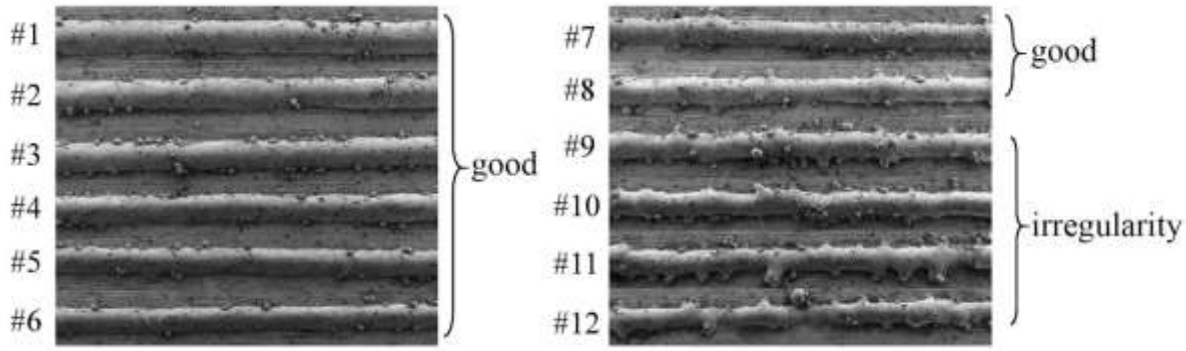

Fig.2 Track morphologies corresponding to different laser powers

3. Methods

3.1 Feature extraction.

Fig.3 shows a typical image around the melting zone. In the image three objects, i.e. melt pool, plume and spatters, can be clearly observed. To explore the correlations of information extracted from different objects with the process conditions, features were extracted corresponding to the three objects. The details on image processing can be found in our previous work[17]. The features considered in this study include melt pool area v_1, plume area

v_2, plume orientation v_3 ($v_3 = \phi$), spatter orientation v_4 ($v_4 = \sum \theta_i / v_5$, θ_i is the orientation of each spatter), the number of spatters (v_5), and spatter dispersion index ($v_6 = \sqrt{\frac{\sum (\theta_i - v_4)^2}{v_5}}$).

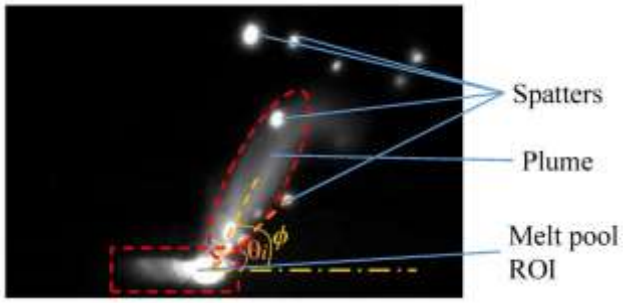

Fig.3 A detected typical optical emission image.

3.2 K-means clustering

K-means clustering partitions is a set of observations ($\boldsymbol{x}_1, \boldsymbol{x}_2, \mathrm{L}\ , \boldsymbol{x}_N$) extracted from the data into *K* mutually exclusive clusters ($C_1, C_2, \mathrm{L}\ , C_K$), and returns a vector of indices which indicate to which of the *K* clusters each feature set has been assigned such that to minimize the sum of distances between each data point x_{ij} and the cluster center μ_k of the subset C_k which contains x_{ij}. Thus, the objective is to find:

$$\arg\min \sum_{i=1}^{K} \sum_{j=1}^{M} d(x_{ij}, \mu_i) \tag{1}$$

where *K* is the number of observations of the cluster C_i, x_{ij} is the *j*th observation of the *i*th cluster and μ_i is the center of the *i*th cluster which is defined as

$$\mu_i = \frac{1}{M} \sum_{j=1}^{M} x_{ij}, \quad i = 1, \mathrm{L}\ , K \tag{2}$$

$d(x_{ij}, \mu_i)$ is a distance measured between the data point and the cluster centroid. The distance measure used in this study is the Euclidean distance which measures the straight line distance between two data points.

$$d(x_{ij}, \mu_i) = \sqrt{(x_{ij} - \mu_i)^2} \tag{3}$$

The steps for the implementation of *K*-means clustering is as follows:

1) Determine the number of clusters *K*,
2) Initialize the centroids of the *K* clusters,
3) Calculate the Euclidean distance between data points and each cluster centroid,

4) Assign each data point to the nearest cluster,
5) Recalculate the new centroids of the modified clusters, and
6) Repeat step 3 until the centroids are stable.

3.3 Support vector machine

Support vector machine (SVM) is a well-known and popular method in classifying applications. It has an outstanding generalization performance based on the structural risk minimization principle [18, 19]. Let $\mathrm{x} = \{x_i, i = 1,2,\mathrm{K}\ ,N\}$ be the feature vectors of the training set, which belongs to two classes. The goal is to design a hyperplane to maximize the margin between two classes, as shown in Fig.4. The hyperplane equation is expressed as,

$$f(x) = w^T \mathrm{x} + b = 0 \tag{4}$$

where x is the input feature vector, y_i is the corresponding class label, w is an adjustable weight vector, and b is a bias. The optimization problem is to find the objective function,

$$\text{minimize } \frac{1}{2}\|w\|^2 + C\sum_{i=1}^{N}\xi_i \tag{5}$$

$$\text{subject to } \begin{array}{ll} y_i(w^T x_i + b) \geq 1 - \xi_i, & i = 1,\mathrm{L}\ ,N \\ \xi_i \geq 0, & i = 1,\mathrm{L}\ ,N \end{array}$$

where ξ_i is to measure the distance between the margin and the examples x_i which locate on the wrong side of the margin, and C is the user-defined penalty for error.

By introducing a set of Lagrange multipliers, the calculation can be converted to a dual optimization problem,

$$\text{maximize } Q(a) = \sum_{i=1}^{N}\alpha_i - \frac{1}{2}\sum_{i=1}^{N}\sum_{j=1}^{N}\alpha_i\alpha_j y_i y_j x_i^T x_j \tag{6}$$

$$\text{subject to } \sum_{i=1}^{N}\alpha_i y_i = 0 \text{, and } 0 \leq \alpha_i \leq C \text{ for } i = 1,2,\mathrm{K}\ ,N$$

where α_i is Lagrange multiplier. Then the decision function is,

$$g(x) = sign(\sum_{i,j=1}^{N}\alpha_i y_i x_i x_j + b) \tag{7}$$

Though SVM was originally introduced for linear classification, it can efficiently perform a nonlinear classification using the kernel, and implicitly mapping their inputs into high-dimensional feature spaces. With the kernel function, the Eq. (2) can be expressed as,

$$Q(a) = \sum_{i=1}^{N}\alpha_i - \frac{1}{2}\sum_{i=1}^{N}\sum_{j=1}^{N}\alpha_i\alpha_j y_i y_j k(x, x_i) \tag{8}$$

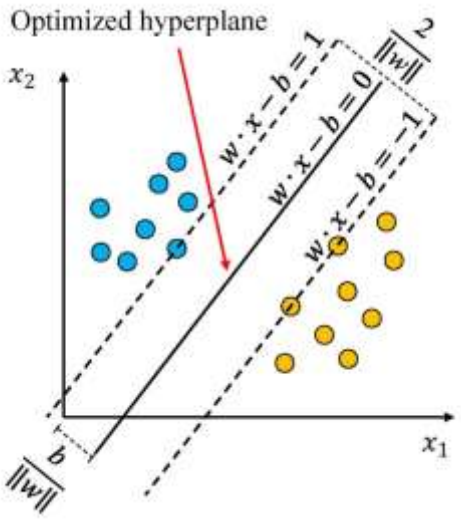

Fig.4 The schematic of support vector machine

4. Results and Discussion

4.1 Influence of laser power on extracted features

Fig.5 shows the detected features of a track built by different laser powers. In the cases of "*good*" track built (laser power >100 W), the detected melt pool area and the plume area both increase with laser power. This can be explained by the commonly known process mechanism that the metal powders absorb laser energy and melt along with temperature increase, thus, using a higher laser power means more powders will be melt and the melt pool will be vaporized easier. However, in the cases of "*irregularity*" track built (laser power ≤100 W), the variation trends of the melt pool area and the plume area are inconsistent with the interpretation of this physical process, and the melt pool area and the plume area are both relatively higher compared with those larger than 100 W. Moreover, the variances of the melt pool area and the plume area become larger when the laser power is lower than 100 W. To find out the reason for this anomaly, the videos recorded were observed and analyzed. It was found that using laser power smaller than 100 W, the metal powders closed to the melt pool would be vaporized frequently, forming a high brightness and large plume. Meanwhile, this plume lights up the melt pool, as a result, the detected melt pool area is larger than the true melt pool area, as shown in Fig.6. As seen in Fig.2, the track morphology presents irregularity in the cases of laser power smaller than 100 W. This indicates that the track irregularity maybe caused by the vaporization of the powders closed to the melt pool, as pressure will be built up on the melt pool due to this vaporization and it may disturb the stability of the melt pool. Additionally, this illustrates that the powder vaporization phenomenon will bring significant deviation in melt pool profile detection by using the optical emission in NIR waveband, especially in the irregularity regime.

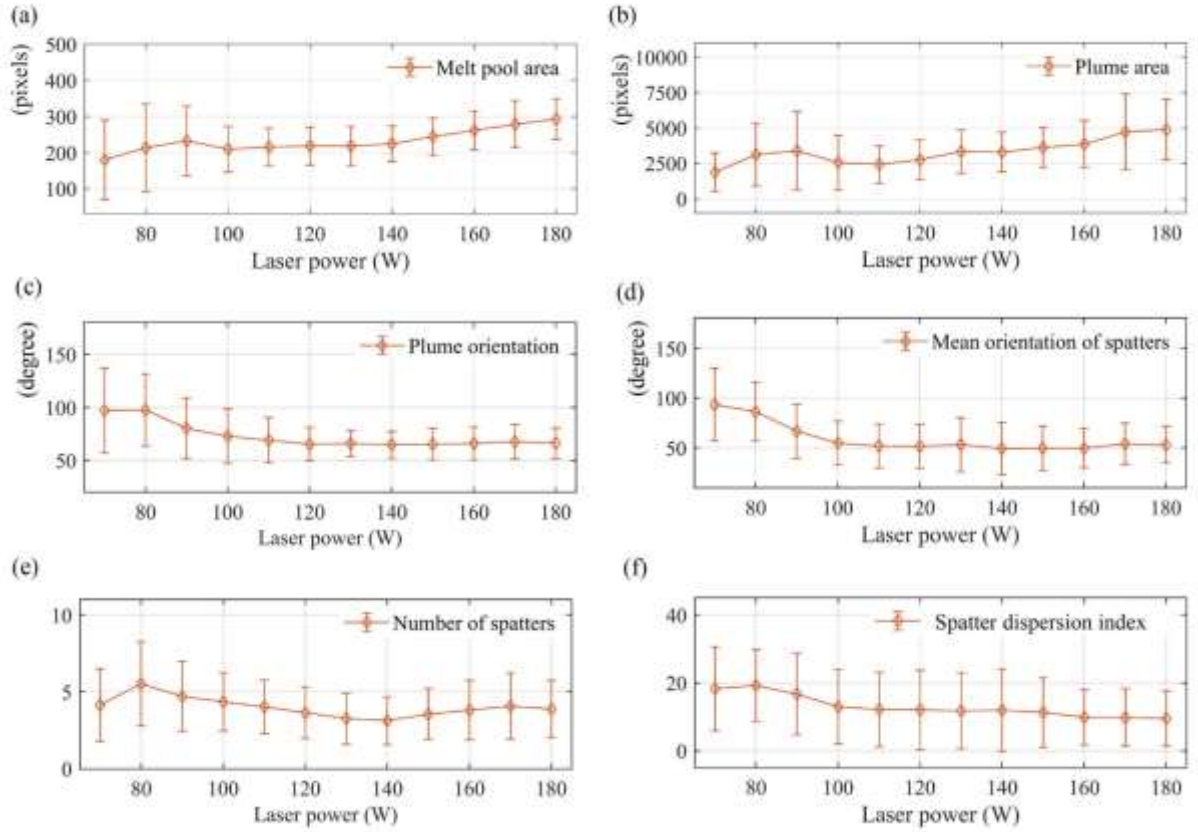

Fig.5 The detected features of track built by different laser powers

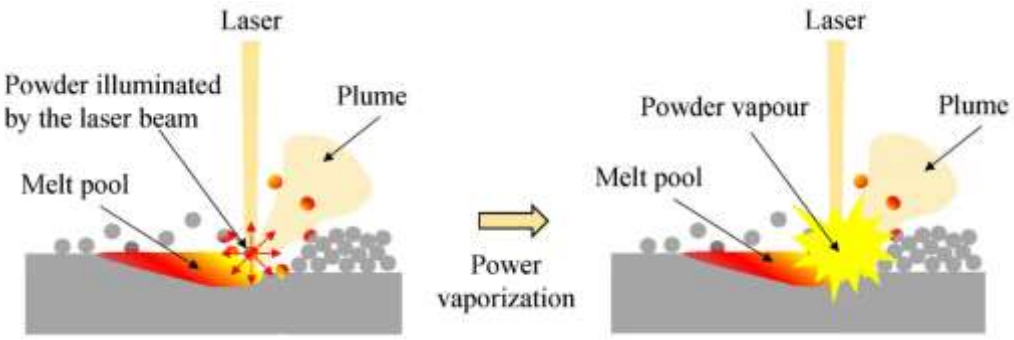

Fig.6 Vaporization of the powder illuminated by the laser beam

When the laser power is higher than 100 W, the plume orientation does not show significant changes. When the laser power is lower than 100 W, the plume orientation increases with the decrease of laser power, and the variance of plume orientation presents noticeable increases. Moreover, in some cases the plume orientation is larger than 90°, and in other cases the plume orientation is smaller than 90°. This illustrates that the plume orientation varies between forward and backward frequently when the laser power is insufficient. The variation trend of spatter orientation is consistent with the plume orientation, this is because the majority of the spatters are generated by the gas entrainment phenomenon [20]. Consequently, spatter ejected direction is consistent with the vapor plume ejected direction. However, the variances of spatter

orientation are high for all laser powers as studied in this work, and this maybe because several spatters are detected in an image and the spatter orientation presents in Fig.5 (d) is the average orientation of these spatters. Fig.5(e) shows the change of number of spatters with laser power. For the laser power of 140 W, the number of spatters is minimum. When the laser power becomes higher or lower, the number of spatters both increases, which is consistent with the experiment result in [16]. Based on our observation, the causes of generating more spatters are different for the two cases of higher and lower laser power. In the case of higher laser power, the melt pool surface vaporization becomes intense leading to more spatters ejected. In the case of lower laser power, the plume vapor ejected direction becomes vibrant, thus, its affected region increases resulting in more spatters ejected, as shown in Fig.7.

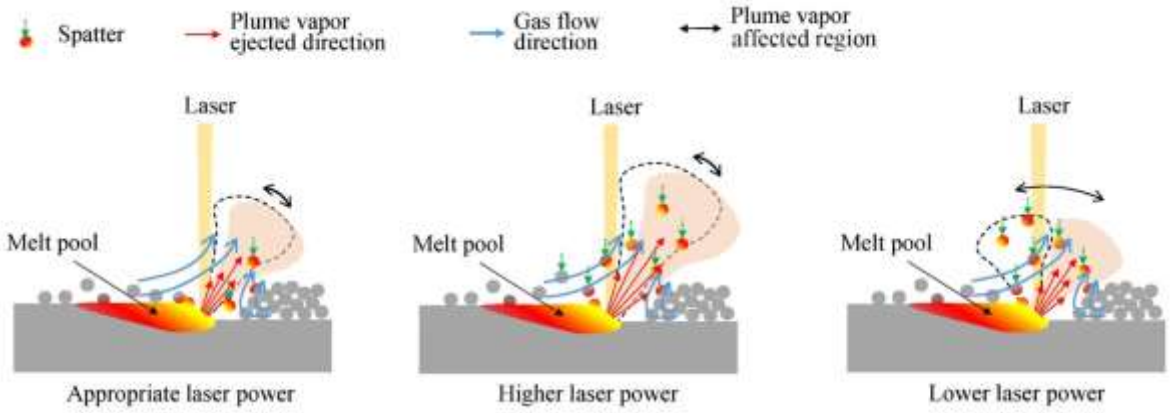

Fig.7 The schematic of the causes of more spatters generated with higher laser power and lower laser power.

Beside the number of spatters, a dispersion index is introduced to study the spatial distribution characteristic of spatters. The dispersion index is defined as,

$$c = \sqrt{\frac{\sum(\theta_i - \bar{\theta})^2}{N}} \tag{9}$$

where θ_i is the orientation of the ith spatter in an image, $\bar{\theta}$ is the average orientation of all spatters in the image, N is the number of spatters. This dispersion index decreases with the increase of laser power, as shown in Fig.5 (f). This can be explained as that with the increase of the laser power, the plume vapor ejected velocity increase, leading to the increase of the gas entrainment force. As a result, the spatters are gathered and tend to be ejected in the same orientation with the plume vapor.

4.2 Clustering Analysis

Based on the above analysis, the extracted features show some variation trends with the laser power and they can be explained by the process physical mechanisms, which indicates they have the potential in process condition detection. However, the high error bars in Fig.5 shows that it is quite challenging to detect the process condition based on any individual feature. As the six features mentioned above will all be affected by the laser power, it can be assumed that

maybe there are some hidden patterns among these features that can be used for process condition detection. To verify the assumption, the clustering analysis of these features were conducted in the following.

To find out the hidden patterns, the *K*-means clustering method was adopted in the study. *K*-means clustering analysis partitions the features into a number of clusters with the aim of maximizing the similarities of the observations in the same cluster while minimizing those between clusters[21]. It is an easy and effective clustering analysis methods, which is commonly used for data analysis, mechanisms discovery and classification[22]. The two key points for *K*-means clustering method is to determine the number of clusters and the initial centroids for each cluster, which is detailed in the following sections.

4.2.1 Feature selection

In order to improve clustering efficiency and quality, feature selection is necessary to remove the irrelevant and redundant information. Laplacian score [23], an advanced variance analysis method, was adopted in the study for unsupervised feature selection. Fig.8 shows the average Laplacian score of each feature. It can be seen that the average Laplacian score for all the features are larger than 0.9, which indicates that they all have good capability of clustering.

To reduce the redundancy of data, feature selection based on data correlation was also conducted. Table 2 compares the correlation coefficient of the features, the value of correlation coefficient of v_1 and v_2, v_3 and v_4 are clearly higher than the others. This indicates that v_1 and v_2, v_3 and v_4 are correlated, while v_5 and v_6 are more independent which are suitable for clustering. As the Laplacian score of v_2 is higher than v_1, and v_3 is higher than v_4, v_2 and v_3 are selected for clustering. In summary, the selected features for clustering are v_2, v_3, v_5 and v_6, i.e. plume area, plume orientation, number of spatters, and spatter dispersion index.

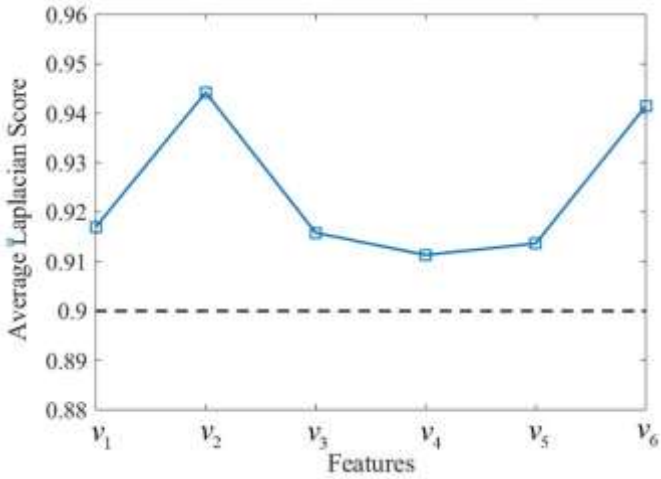

Fig.8 Feature selection using average Laplacian score for the features

Table 2: correlation coefficient of the descriptors

	v_1	v_2	v_3	v_4	v_5	v_6
v_1	1	**0.4744**	-0.2581	-0.3225	-0.1040	-0.1107
v_2	0.4744	1	-0.0252	-0.0102	0.0293	0.0593
v_3	-0.2581	-0.0252	1	**0.5009**	0.1470	0.2726

v_4	-0.3225	-0.0102	0.5009	1	0.1927	0.2751
v_5	-0.1040	0.0293	0.1470	0.1927	1	0.2049
v_6	-0.1107	0.0593	0.2726	0.2751	0.2049	1

4.2.2 Initialization of cluster centroids

The *K*-means clustering algorithm is sensitive to the initial positions of the centroids. To obtain a good final cluster structure the *K*-means++ algorithm is adopted for cluster centroid initialization. *K*-means++ algorithm was proposed by David in 2007 [24]. They demonstrated their initialization algorithm improves both the speed and the accuracy of the standard *K*-means method. Let $D(x)$ denote the shortest distance from a data point x to the closest centroid already selected. The *K*-means++ initialization algorithm is described as follows. Firstly, select a data point uniformly at random from the data set *X* as the first initial centroid c_1; then select the next centroid c_i at random from *X* with probability $\frac{D(x')^2}{\sum_{x\in X} D(x)^2}$, that is, to select each new centroid with a probability proportional to the distance from itself to the closest centroid that we already selected. Repeat this step until the *k* centroids are selected.

4.2.3 Selection of number of clusters

To determine the number of clusters, two indices were used for clustering validity evaluation, which are Silhouette coefficient[25] and Davies-Bouldin index[26]. Silhouette coefficient combines ideas of both cohesion and separation, measuring the separability of the clusters. The Silhouette coefficient for an individual point is described as:

$$SC = \frac{1}{N}\sum_{i=1}^{N}\frac{b(x)-a(x)}{\max\{a(x),b(x)\}} \tag{10}$$

where $a(x)$ denotes the distance of point x to the other points in the same cluster, $b(x)$ denotes the distance of point x to the points in the other clusters. The value of *SC* is higher for well-separated clusters.

The Davies-Bouldin (D-B) index is a function of the ratio of within-cluster and between-cluster distances, which is described as

$$DB = \frac{1}{k}\sum_{i=1}^{k}\max\{D_{i,j}\}, \quad \mathrm{D}_{i,j} = \frac{\bar{d}_i + \bar{d}_j}{d(c_i,c_j)} \tag{11}$$

where $\bar{d}_i$ is the average distance between each point in the *i*th cluster and the centroid of the *i*th cluster. $\bar{d}_j$ is the average distance between each point in the *i*th cluster and the centroid of the *j*th cluster. $d(c_i,c_j)$ is the Euclidean distance between the centroids of the *i*th and *j*th cluster. The clustering algorithm is considered better with a smaller Davies-Bouldin index.

Fig.9 shows the mean Silhouette value and Davies-Bouldin index for a cluster number in the range of 2 to 10. Based on this result, number of 5 is selected as the optimized cluster number.

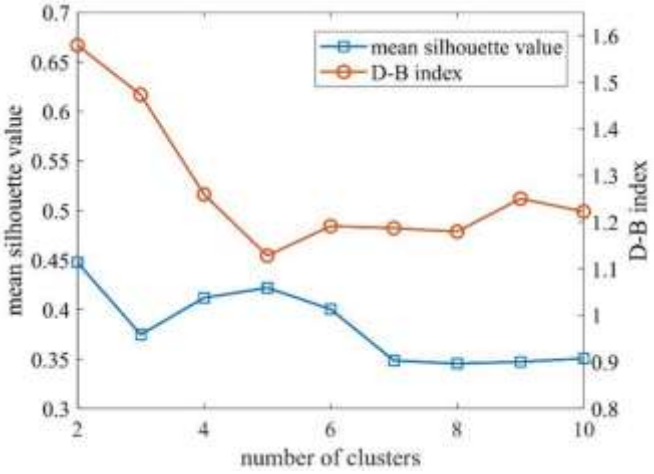

Fig.9 The number of clusters evaluated by Silhouette coefficient and Davies-Bouldin (D-B) index

4.2.4 Cluster analysis

To better cluster and visualize the clusters, principle component analysis (PCA) [27] was used to project the selected feature vector $v = [v_2\ v_4\ v_5\ v_6]$ in section 4.2.1 on the new coordinates, which are principal components (PCs), with maximum variance in the data set. Fig.10 presents the projection of the four clusters to 3-dimensional plot by three principal components. It is clear that the extracted features are separated. Table 3 shows the percentage of data points in each cluster. 39.91% data points are partitioned in cluster-2, which is much higher than the other four clusters.

Fig.11 shows the visualization of *K*-means clustering prediction for the tracks built by different laser powers. It can be seen in the range of laser power higher than 100 W, the prediction results located in cluster-2 are more than in the range of laser power lower than 100 W. This indicates that the cluster-2 is the dominant pattern for "good" track fabrication. In the whole range of laser power studied, there are some prediction results located in cluster-3 and cluster-4, and they do not present any distribution regularities. In the range of low laser power, the number of prediction results located in cluster-5 increases with the decrease of laser power. This illustrates that the cluster-5 may be the pattern that is responsible for the built quality degradation. It is worth noting that the pattern of cluster-1 occurs frequently in the cases of both high laser power and low laser power, but rarely occurs in the middle range of the studied laser powers. The reason is detailed in the following discussion.

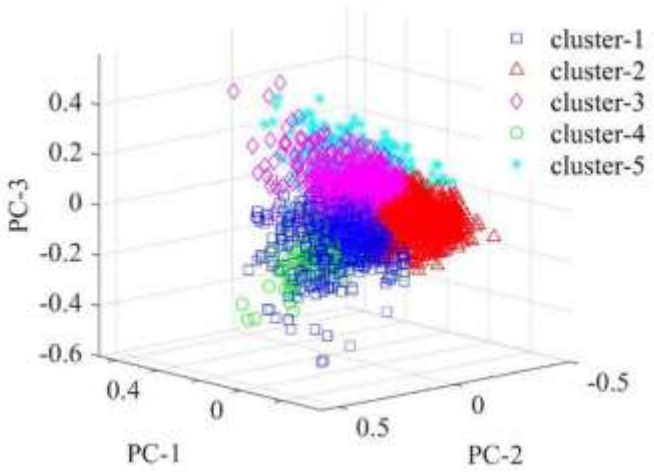

Fig.10 PCA visualization of *k*-means clustering of the extracted features

Table 3: Percentage of data points in each cluster

	cluster-1	cluster-2	cluster-3	cluster-4	cluster-5
Percentage (%)	14.26	39.91	25.21	12.06	8.57

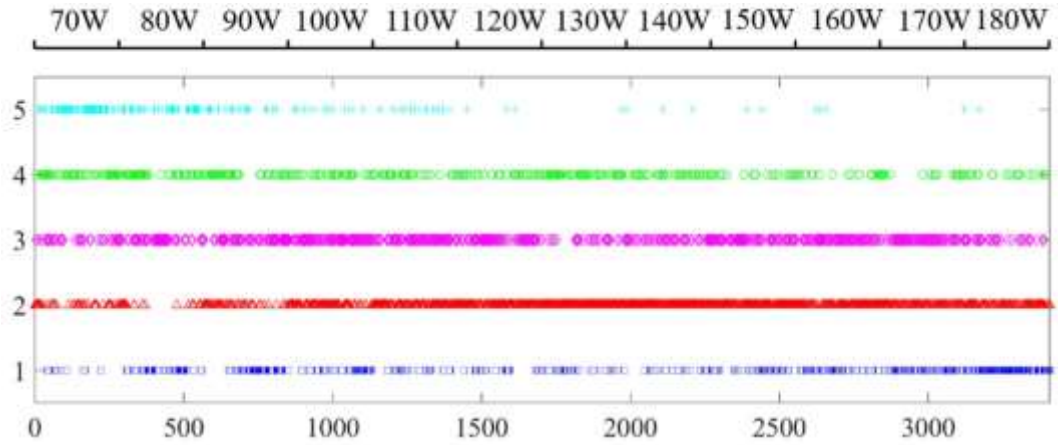

Fig.11 Visualization of *k*-means clustering prediction for tracks built by different laser powers

To further visualize the traits of the features selected for clustering, the distribution of the features in each cluster is shown in Fig.12. The plume area is significantly higher in cluster-1 than the others. And a boundary can be identified in the range of plume area between 5,000 and 6,000 pixels. This indicates that the melt pool will be remarkably vaporized in this cluster. For cluster-2, cluster-3 and cluster-4, the plume area distributions are quite similar, mainly in the range of 1,000 to 5,000 pixels. And for cluster-5 the plume area is relatively low, that is why more prediction results located in cluster-5 in the range of low laser power, as shown in Fig.11.

As shown in Fig 12 (b), the distributions of plume orientation for cluster-1, cluster-2, cluster-3 and cluster-4 are quite similar. Among them the central value of cluster-1 is lightly higher.

The distribution of plume orientation for cluster-5 is different from the others, mainly in the range that higher than 100°. As the plume orientation is defined as the angle between the plume ejected direction and the laser scanning direction, when the plume orientation is less than 90º the plume is ejected forward, otherwise, the plume is ejected backward. Therefore, it can be concluded that the plume is ejected backward in cluster-5 and forward in other clusters.

As shown in Fig.12 (c), for cluster-1 and cluster-5 the distributions of the number of spatters are similar and close to normal distributions. For cluster-2 and cluster-3 generally less than 5 spatters are generated, while for cluster-4 generally more than 5 spatters are generated.

As shown in Fig.12 (d), the spatter dispersion index is remarkably higher in cluster-3 than cluster-1, cluster-2 and cluster-4. A boundary can be identified in the range of spatter dispersion index between 19 and 21. This illustrates that the spatter spatial distribution in the image is quite scattering for cluster-3. For cluster-5 the spatter dispersion index is likely to be in any subranges, which reveals that the spatter dispersion index is not an essential indicator for cluster-5 identification.

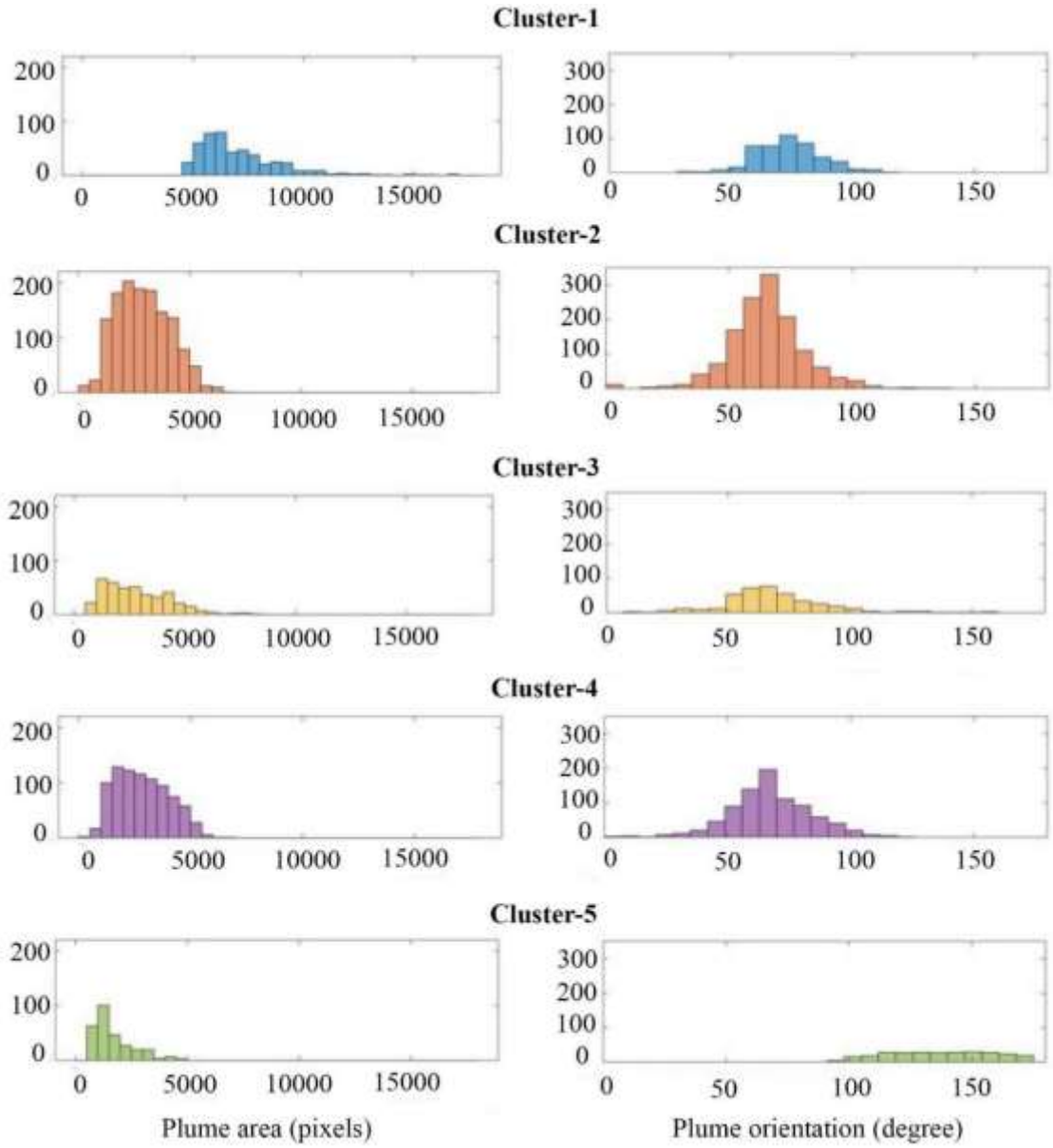

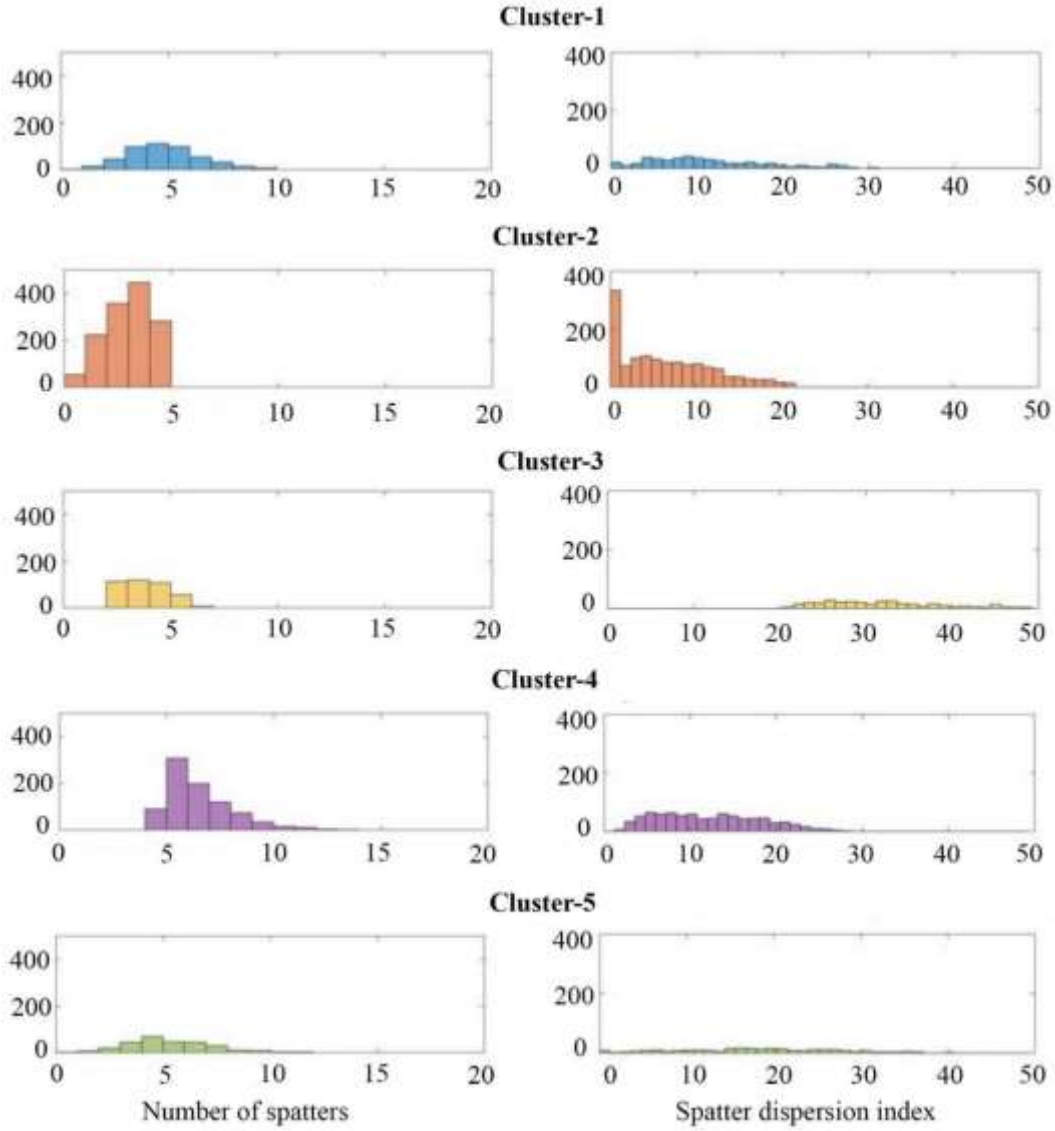

Fig.12 The extracted descriptors distribution in each cluster

The processing traits of the five clusters can be described as follows. For cluster-1, the plume is ejected forward, thus the plume area is large; some spatters are ejected in a roughly same direction; for cluster-2, the plume is ejected forward, the plume area is in an appropriate range, fewer spatters are ejected and they are also ejected in a roughly same direction; for cluster-3, the plume is ejected forward, the plume area is in an appropriate range, fewer spatters are ejected but the spatial distribution of the spatters is highly scattering; for cluster-4, the plume is ejected forward, the plume area is still in an appropriate range, more spatters are ejected and their ejected direction is roughly same; for cluster-5, the plume is ejected backward, the plume area is small, some spatters are ejected and their ejected direction shows no regularities.

Therefore, it can be concluded that the difference between cluster-2 and cluster-3 is that the spatial distribution of spatters is scattering in cluster-3 but is agminated in a roughly same direction in cluster-2. The difference between cluster-2 and cluster-4 is that more spatters are ejected in cluster-4 than cluster-2. As cluster-2 is identified as the dominant pattern for normal process condition, the pattern of cluster-3 and cluster-4 are quite close to the normal process condition. The generation of more spatters or the scattering spatial distribution of spatters

maybe caused by little vibrations during the process. As shown in Fig.11, the pattern of cluster-3 and cluster-4 frequently occur in the cases of "good" track built. This reveals that it is difficult to achieve an absolute stable built in SLM process as its physical process is quite complex. However, some small vibrations will not bring serious consequences on built quality. The process cannot be identified as unstable if only more spatters are detected or the detected spatters shows a scattering spatial distribution.

The difference between cluster-2 and cluster-1 is that the plume area is significantly larger in cluster-1. In the range of high laser power, the occurrence number of cluster-2 increases with the increase of laser power (Fig.11). It is worth noting that the occurrence number of cluster-2 in laser power range from 80W to 100W is also high. This is because the detected plume area could be very high due to the powder vaporization phenomenon, as shown in Fig.6. Thus, only using plume area as the indicator for process condition detection is difficult to determine that the anomaly is caused by high energy input or insufficient energy input.

The cluster-5 shows the biggest differences from the cluster-2. First, the plume is ejected backward in cluster-5 but forward in cluster-2. Second, the plume area is smaller in cluster-5. In addition, the spatial distribution spatters in cluster-5 is possible to be agminated in a same direction or to be highly scattering. Therefore, the cluster-5 should be easier to be identified based on the detected information. As shown in Fig.10, the occurrence of cluster-5 is mainly in the range of low laser power, and the occurrence number increases with the decrease of laser power. This shows that cluster-5 is an effective indicator to detect the quality degradation caused by insufficient energy input.

In summary, in PBF process the optical emission features have a dominant pattern in a "good" process condition. Some minor process vibrations may cause variations on the detected features, such as the increase of the number of spatters and the increase of the spatter dispersion index. However, the weak process vibrations have little effect on built quality. Two patterns of the features, cluster-1 and cluster-5, are identified and should be responsible for the degradation of track quality. Moreover, it is found that the plume area and the plume orientation are the most important indicators for the identification of cluster-1 and cluster-5, respectively. Meanwhile, it is worth noting that the cluster-5 occurs frequently both in the cases of quality degradation and in the cases of high energy input. Therefore, using plume area has limitation on quality degradation identification.

4.3 *Supervised learning for track quality identification*

As discussed above, five patterns of melt pool condition could occur in the PBF process, and the melt pool condition frequently changes among these patterns. The occurrence of any individual pattern is insufficient for quality identification as the track built is the result of the accumulation of melt pool dynamic process. Therefore, to identify the built quality the melt pool information in time series should be considered. Based on the observation of the track morphologies, the track samples are labeled as two groups, that are "good" and "irregularity" (Fig.2). The images recorded during the samples built are used as the dataset to build a supervised learning model for quality identification. The feature vector includes the sequential features extracted from the images, $\mathbf{V} = [\mathbf{v}_1^T, \mathbf{v}_2^T, \mathrm{L}\ , \mathbf{v}_n^T]^T$. n is the length of time sequence, $\mathbf{v}_i$ is the feature vector of the ith time sequence. The support vector machine (SVM) method is adopted for supervised learning model establishment, which is commonly used for pattern

recognition. The kernel used is Gaussian kernel, and 5 folds is used for cross-validation. In the study two SVM models are built based on different features. The feature vector $\mathbf{v}$ for SVM-1 model includes only two feature variables, i.e. plume area (v_1) and plume orientation (v_2), which are the most crucial ones for quality degradation identification based on the clustering analysis. The feature vector $\mathbf{v}$ for SVM-2 model includes the four feature variables selected for clustering, plume area (v_1), plume orientation (v_2), spatter orientation (v_3) and spatter dispersion index (v_4). Fig.13 shows the validation accuracy of the SVM models with different length of time sequence.

It can be seen that with the increase of the length of sequence the validation accuracy both increases significantly at the beginning and later tends to be stable for the two SVM models. It demonstrates that the information in time sequence can help improve the quality identification performance. Additionally, the validation accuracy of the SVM-2 model is higher than the SVM-1 model, but the SVM-1 model still can obtain a good accuracy. It is higher than 85% when the features in more than 4 sequences are used for classification. This illustrates that with the two most crucial features a good quality identification result can be obtained, and with more features the quality identification performance can be further improved. However, using more features means more time is needed for data processing, which is challenging for an online monitoring application. Therefore, the two features, plume area and plume orientation are highly recommended for quality monitoring considering the balance between the classification accuracy and the time needed for data processing.

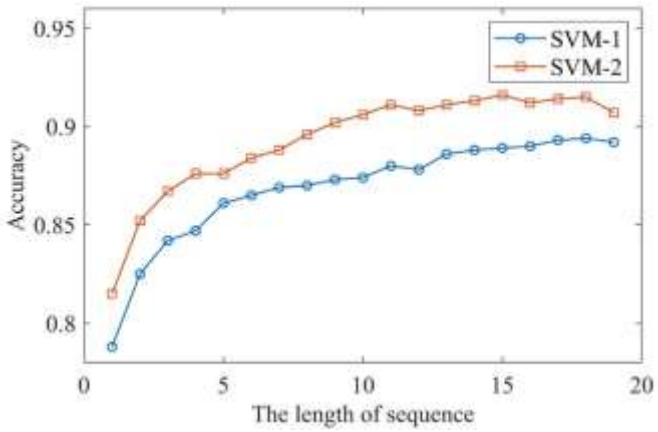

Fig.13 The validation accuracy of the SVM models with different lengths of time sequence.

5. Conclusions

A high-speed camera is used to acquire the PBF process images. The cut-off filter is configured to make it sensitive to the waveband of 800nm-1000nm. The features of melt pool area, plume area, plume orientation, spatter orientation, number of spatters and spatter dispersion index were extracted from the images recorded. The variations of these features with the increase of laser power is investigated. The mean value of these features shows different trends with laser power, which is explained based on process physical mechanisms and our observations. The high variance of any individual feature makes it not suitable for process condition monitoring.

The *K*-means clustering method was used to discover the hidden patterns of these features. The collected dataset was partitioned into five patterns. The typical pattern under "good" process condition is identified. Pattern-1 and pattern -5 which frequently occur in the cases of low laser are responsible for the built quality degradation. The features in each pattern is characterized. It is found that high plume area is the crucial element for the pattern-1 identification, and high plume orientation is the crucial element for the pattern-5 identification. Therefore, they are the two crucial features for quality degradation detection. In addition, the number of spatters and the spatter dispersion index are found sensitive to some minor process vibrations which have little effect on built quality. Moreover, the occurrence of pattern-1 both increase in the case of using high laser power and low laser power. Thus, it is insufficient to determine the quality condition based on the occurrence of high plume area. A supervised learning model based on SVM algorithm is established based on the features extracted to distinguish the "good" and "irregularity" tracks built. The results show that the time sequence information is crucial to improve the quality identification performance. And the two features, i.e. plume area and plume orientation are highly recommended for process quality identification considering the balance between the identification accuracy and time needed for data processing. These findings give insight into the optical emission in the PBF process and provide guidelines for process monitoring system development.

Acknowledgement:

The authors would like to acknowledge the multiple supports from China Scholarship Council, South China University of Technology (SCUT) and National University of Singapore (NUS).

Ethical Approval:

Not appliable.

Consent to Participate:

Not appliable.

Consent to Publish:

Not appliable.

Authors Contributions:

Yingjie Zhang design the experiment, analyze the data and write the paper. Wentao Yan helps improve the idea and experiment design. Xiaojun Peng helps collect and analyze the data. Zhangdong Chen and Zimeng Jiang help collect the data. Di Wang provides experiment equipment and helps improve the data analyses part.

Funding:

The work is supported by the National Key R&D Program of China (grant No. 2021YFE0203500).

Competing Interests:

The authors declare that they have no competing interests.

Availability of data and materials:

All data generated or analyzed during this study are included in the paper.

References:

[1] Mani, M., Feng, S., Lane, B., Donmez, A., Moylan, S., and Fesperman, R., 2015, Measurement science needs for real-time control of additive manufacturing powder bed fusion processes, US Department of Commerce, National Institute of Standards and Technology.
[2] Spears, T. G., and Gold, S. A., 2016, "In-process sensing in selective laser melting (SLM) additive manufacturing," Integrating Materials and Manufacturing Innovation, 5(1), p. 2.
[3] Grasso, M., and Colosimo, B. M., 2017, "Process defects and in situ monitoring methods in metal powder bed fusion: a review," Measurement Science and Technology, 28(4), p. 044005.
[4] Craeghs, T., Clijsters, S., Kruth, J.-P., Bechmann, F., and Ebert, M.-C., 2012, "Detection of process failures in layerwise laser melting with optical process monitoring," Physics Procedia, 39, pp. 753-759.
[5] Craeghs, T., Bechmann, F., Berumen, S., and Kruth, J.-P., 2010, "Feedback control of Layerwise Laser Melting using optical sensors," Physics Procedia, 5, pp. 505-514.
[6] Clijsters, S., Craeghs, T., Buls, S., Kempen, K., and Kruth, J.-P., 2014, "In situ quality control of the selective laser melting process using a high-speed, real-time melt pool monitoring system," The International Journal of Advanced Manufacturing Technology, 75(5-8), pp. 1089-1101.
[7] Grasso, M., Laguzza, V., Semeraro, Q., and Colosimo, B. M., 2017, "In-process monitoring of selective laser melting: spatial detection of defects via image data analysis," Journal of Manufacturing Science and Engineering, 139(5), p. 051001.
[8] Repossini, G., Laguzza, V., Grasso, M., and Colosimo, B. M., 2017, "On the use of spatter signature for in-situ monitoring of Laser Powder Bed Fusion," Additive Manufacturing, 16, pp. 35-48.
[9] Grasso, M., Demir, A., Previtali, B., and Colosimo, B., 2018, "In situ monitoring of selective laser melting of zinc powder via infrared imaging of the process plume," Robotics and Computer-Integrated Manufacturing, 49, pp. 229-239.
[10] Zhang, Y., Hong, G. S., Ye, D., Zhu, K., and Fuh, J. Y., 2018, "Extraction and evaluation of melt pool, plume and spatter information for powder-bed fusion AM process monitoring," Materials & Design, 156, pp. 458-469.
[11] Montazeri, M., and Rao, P., 2018, "Sensor-Based Build Condition Monitoring in Laser Powder Bed Fusion Additive Manufacturing Process Using a Spectral Graph Theoretic Approach," Journal of Manufacturing Science and Engineering, 140(9), p. 091002.
[12] Scime, L., and Beuth, J., 2019, "Using machine learning to identify in-situ melt pool signatures indicative of flaw formation in a laser powder bed fusion additive manufacturing process," Additive Manufacturing, 25, pp. 151-165.

[13] Hussein, A., Hao, L., Yan, C., and Everson, R., 2013, "Finite element simulation of the temperature and stress fields in single layers built without-support in selective laser melting," Materials & Design (1980-2015), 52, pp. 638-647.
[14] Li, Y., and Gu, D., 2014, "Parametric analysis of thermal behavior during selective laser melting additive manufacturing of aluminum alloy powder," Materials & Design, 63, pp. 856-867.
[15] Liu, Y., Yang, Y., Mai, S., Wang, D., and Song, C., 2015, "Investigation into spatter behavior during selective laser melting of AISI 316L stainless steel powder," Materials & Design, 87, pp. 797-806.
[16] Gunenthiram, V., Peyre, P., Schneider, M., Dal, M., Coste, F., Koutiri, I., and Fabbro, R., 2018, "Experimental analysis of spatter generation and melt-pool behavior during the powder bed laser beam melting process," Journal of Materials Processing Technology, 251, pp. 376-386.
[17] Zhang, Y., Fuh, J. Y., Ye, D., and Hong, G. S., 2018, "In-situ Monitoring of Laser-based PBF via off-axis Vision and Image Processing Approaches," Additive Manufacturing.
[18] Yin, Z., and Hou, J., 2016, "Recent advances on SVM based fault diagnosis and process monitoring in complicated industrial processes," Neurocomputing, 174, pp. 643-650.
[19] Jing, C., and Hou, J., 2015, "SVM and PCA based fault classification approaches for complicated industrial process," Neurocomputing, 167, pp. 636-642.
[20] Ly, S., Rubenchik, A. M., Khairallah, S. A., Guss, G., and Matthews, M. J., 2017, "Metal vapor micro-jet controls material redistribution in laser powder bed fusion additive manufacturing," Scientific reports, 7(1), p. 4085.
[21] Hartigan, J. A., and Wong, M. A., 1979, "Algorithm AS 136: A k-means clustering algorithm," Journal of the Royal Statistical Society. Series C (Applied Statistics), 28(1), pp. 100-108.
[22] Yiakopoulos, C., Gryllias, K. C., and Antoniadis, I. A., 2011, "Rolling element bearing fault detection in industrial environments based on a K-means clustering approach," Expert Systems with Applications, 38(3), pp. 2888-2911.
[23] He, X., Cai, D., and Niyogi, P., 2006, "Laplacian score for feature selection," Advances in neural information processing systems, pp. 507-514.
[24] Arthur, D., and Vassilvitskii, S., 2007, "k-means++: The advantages of careful seeding," Proceedings of the eighteenth annual ACM-SIAM symposium on Discrete algorithms, Society for Industrial and Applied Mathematics, pp. 1027-1035.
[25] Gutkin, R., Green, C., Vangrattanachai, S., Pinho, S., Robinson, P., and Curtis, P., 2011, "On acoustic emission for failure investigation in CFRP: Pattern recognition and peak frequency analyses," Mechanical systems and signal processing, 25(4), pp. 1393-1407.
[26] Maulik, U., and Bandyopadhyay, S., 2002, "Performance evaluation of some clustering algorithms and validity indices," IEEE Transactions on Pattern Analysis and Machine Intelligence, 24(12), pp. 1650-1654.
[27] Jolliffe, I., 2011, Principal component analysis, Springer.